Modelling Elastic Deformation of Test Masses in LIGO

Mahmuda Afrin Badhan[1], Michael Landry[2], Rick Savage Jr[2], Phil Willems[3]

Initial length calibrations of kilometer-scale gravitational-wave detectors assumed test masses behaved as rigid bodies within the audio detection band (~40Hz-7kHz). Studies done by S. Hild in 2006 [1] on GEO600 test masses depicted deformations in the form of flexure caused by application of local forces. Assessing these surface displacements using the Gaussian beam of the interferometer has shown increasing divergence from the pendulum response for frequencies near and above 1 kHz. Similar behaviour has been observed in LIGO end test masses (ETMs). We have modelled the behaviour of test masses under the influence of sinusoidally varying forces using the finite-element modeling software COMSOL 3.5. A weighted displacement variation due to the flexure is dependent on radial distance of the force application and stiffness of mass. We employ this understanding of test mass flexure to suggest a compensation scheme for the length calibration procedures of LIGO 4km interferometers.

The gravitational-wave detectors operated by LIGO employ cylindrical test masses made of fused silica to survey spacetime and measure the differential arm-length changes observed in the interferometers. These cylindrical test masses are actuated by coil-magnet systems (OSEMs) and photon calibrators, and respond to such pressure. The initial calibration of kilometer-scale detectors assumed these suspended test masses behaved as rigid bodies under the influence of such external forces. Hence the interferometer response models were only aware of the inertial restoration of these test masses, which fall with frequency (Fig. 3), within the detection band of the interferometers (~40Hz – 7kHz).

Studies done by S. Hild in 2006 [1] on the GEO600 test masses found such masses to be experiencing residual deformations when subject to such localized forces. The total effective displacements of the mirror side facing the beam were found to be inconsistent with the sole pendulum response of a rigid body. These non-negligible residuals began showing large discrepancies between the calibration taking them into account and those excluding them in the kHz range. This showed that we could no longer consider test masses as rigid bodies, making it necessary for us to investigate flexure behaviour in the LIGO test masses.

Comparison between the calibration response model and actuation measurements from the S5 data [2] (Fig. 1) revealed discrepancies in the 10-20% range, above 1 kHz, for both LIGO Hanford interferometers. We believe this is the result of the interferometer beam assessing a flexed surface. If such is the case, it would be necessary to initiate some compensation scheme that could account for this behaviour in the existing calibration models. This would allow more accurate interpretations of the signals detected by DARM, yielding more accurate extraction of systems' parameters.

Finite-element modelling using COMSOL

We used COMSOL 3.5 to study the effects of localized forces on Enhanced LIGO end test masses (ETMs). To model the OSEMs and photon pressure, we applied a sinusodially varying force to the flat sides of the cylinder. The range of driving frequencies specified covered the audio detection band. The four OSEM forces were applied to the anti-reflective (AR) side of the optic and the photon pressure forces to the highly-reflective (HR) side (Table 2).

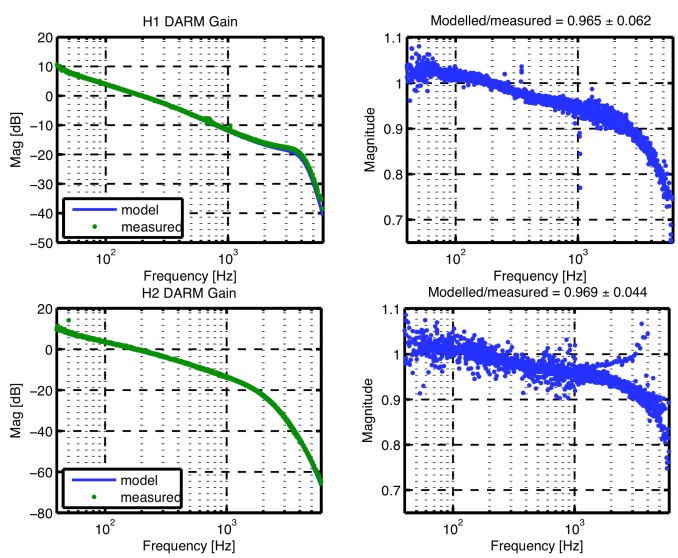

Figure 1| DARM Calibration Data for both H1 and H2 from S5. The ratio begins diverging drastically from 1 at several hundred Hz.

We modelled the individual force configurations using the parameters outlined in Table 2. We then extended this investigation to studying the dependency on slight changes in the radius of the force locales and interferometer beam spot size. The models depicted results for a completely symmetrical test mass with uniform distribution of pressure across the circular force locales.

Our results revealed a definitive presence of surface deformations, which were found be in phase with the center of mass motion, hence adding to the total displacements calculated. On comparing our measured displacements with the pendulum response model, we found that these residuals increase with frequency, especially becoming strong as we approach the drumhead mode at 9537 Hz. This was in accordance with an earlier study carried out by P Willems [3].

[1]Current affiliation: Mount Holyoke College, South Hadley, MA 01075, USA
[2]LIGO Hanford Observatory, Richland, WA 99352, USA
[3]LIGO Project, California Institute of Technology, Pasadena, CA 91125, USA

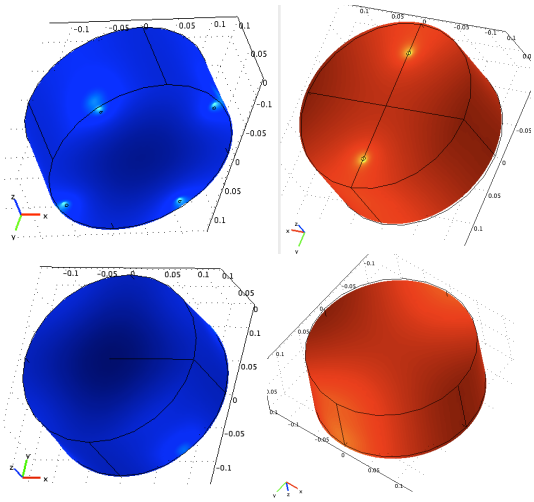

Figure 2| 3D plots showing the force configurations in the individual solved models. The underside (XY plane) is the AR surface. The OSEMs are placed here. The HR surface is actuated by the photon pressure. Red represents positive displacements (z-dir) and blue negative displacements, both of which are out of phase with the respective force configuration.

When four equidistant forces act sinusoidally over the symmetric optic, the quasistatic bending of the optic center is somewhat radially symmetric (Fig. 2). The surface flexure is a combination of raised areas due to the bending and the four dimples produced as a result of the concentrated force distribution. We are only concerned with what the interferometer beam sees at the center of the optic, and so we couple the effective displacements with a Gaussian beam. The overlapping of the beam and the deformation is weighted by a Gaussian intensity distribution, and depends on the spot size ω of the beam.

Assessing mirror flexure near the first internal resonance mode for coil-magnet actuation

At the center of the optic, the HR surface flexure is out of phase with the actuation and thereby, in phase with the free mass motion. Since the bending adds to the motion, the deformation is given by the difference between the total displacement measured and the lower value of the center of mass motion. At the lower frequencies within 1 kHz, we found these deformations to be small enough such that the ratio of this measured motion over the modelled (pendulum) motion is close to 1 (Fig. 4). These residual motions become increasingly significant as we go up the frequency ladder.

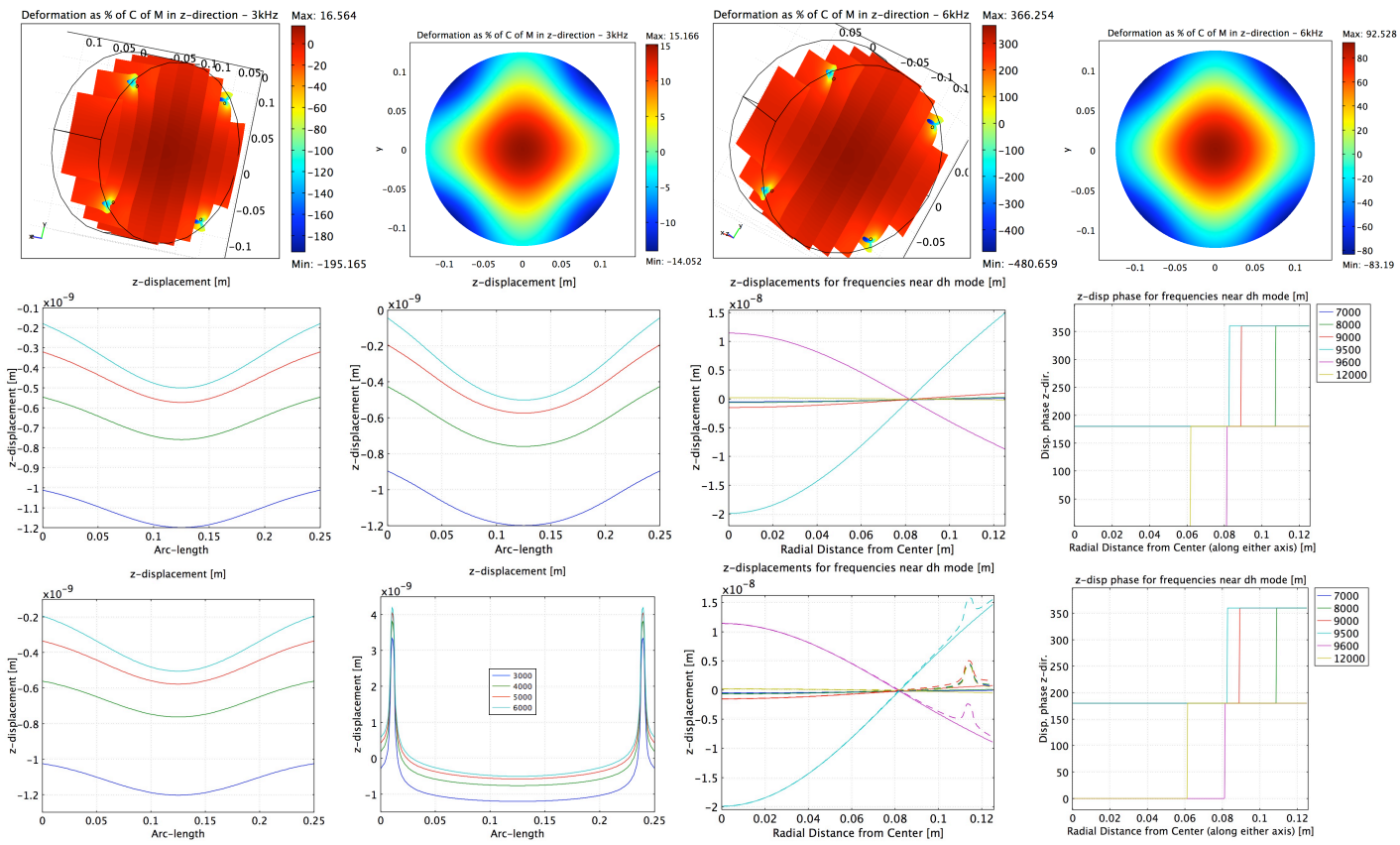

Figure 3| (Top) 2D (AR) and 3D plots of surface deformation in z-direction (perpendicular to optic plane) at 3 kHz and 6kHz respective. (Middle) Line plots of the z-displacements (HR surface) through x (or y) axis and then the diameter over which the forces lie. (Bottom) AR surface version for the previous set of graphs. The first line plot shows results for 3kHz, 4kHz, 5kHz and 6kHz respectively. Second graph focuses on frequencies close to the drumhead mode. The rightmost curve shows the phase relations. The dashed graph represents the near drumhead mode behaviour for a line segment passing through the force locales at the AR surface.

We believe the residual motion is a combination of the mirror flexure, which is found to be almost independent of the driving frequency, and the resonant increase in motion as we approach the maximum amplitudes at the drumhead mode (Fig. 4). Below the first internal resonance mode, the data shows a 10% difference between the measured motion and the center of mass motion, increasing to almost 84% at 6kHz. We did not observe any significant difference between the data for HR and AR surfaces (Fig. 4).

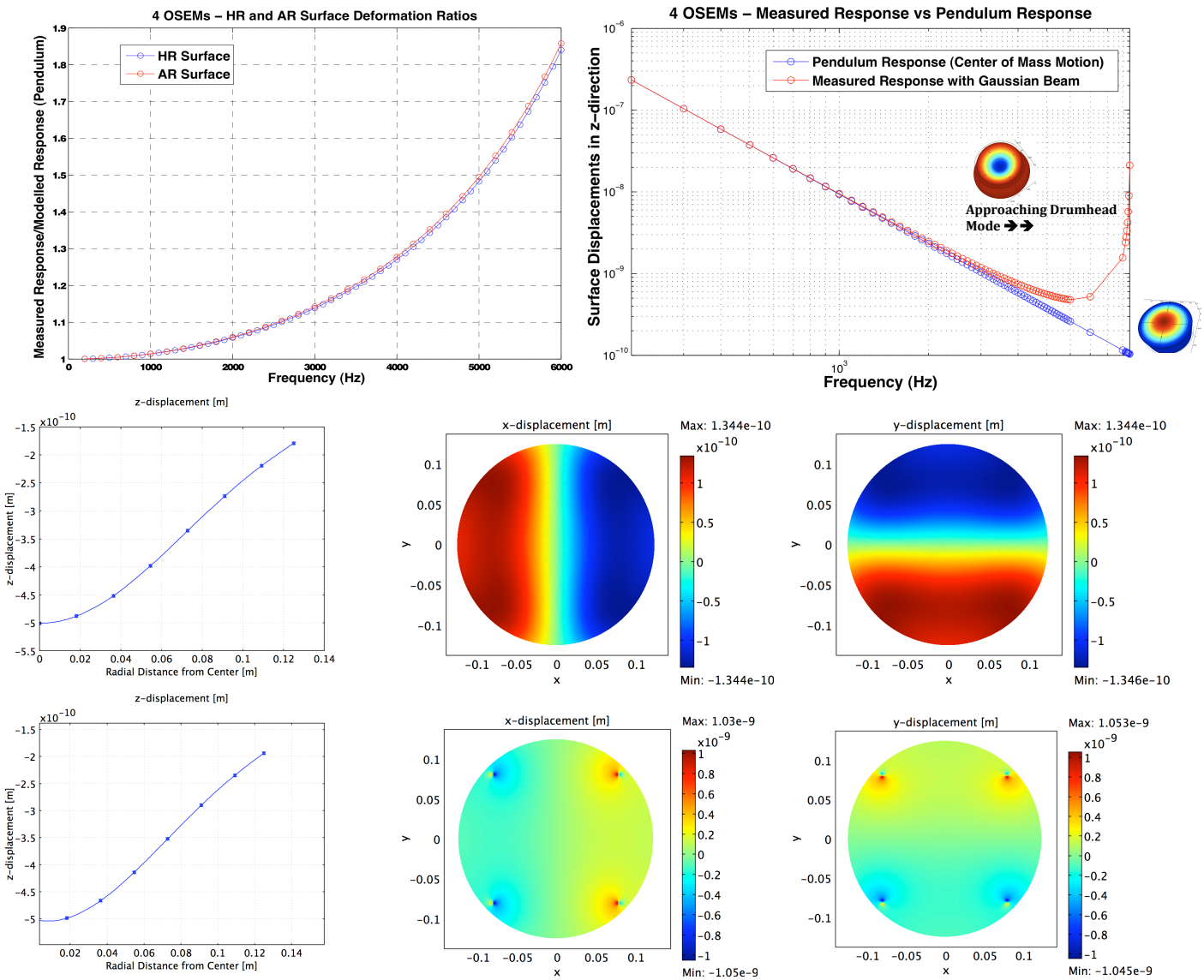

Figure 4| (Top-left) Ratio of the measured response over the modelled (pendulum) response of the center of mass. (Top-right) The measured response as a function of frequency compared with the model response over a larger frequency domain. The lower plots show motion experienced by the optic in x, y, z directions (at 6kHz). The AR surface has expanded slightly, as the result of radial compressions at the HR surface and expansions at the AR surface.

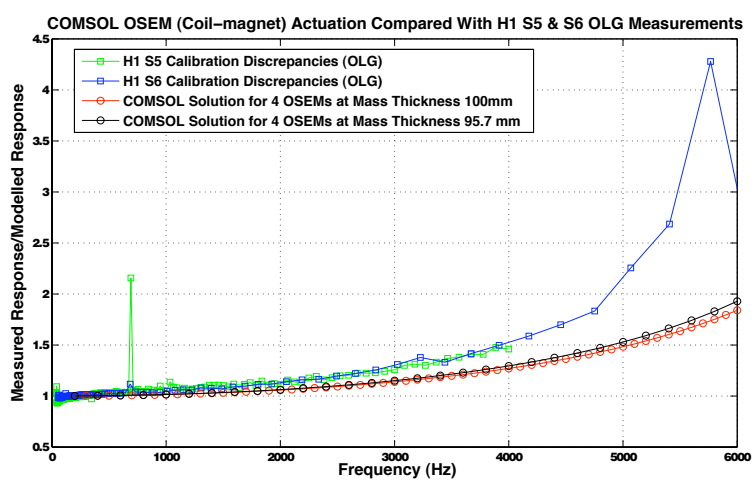

Figure 5| Comparison between the COMSOL modelled results for four OSEM forces and the DARM Calibration Data from S5 and S6. A second set of solutions show the results for a mass thickness of 95.7 mm, which would be the height of the optic if it were to have the same volume as the wedged optic, i.e. the decrease in thickness corresponds to half the vertical length of the wedge. Changing to optic dimensions in such a way changes the diameter-to-thickness ratio, causing the stiffness to change as well.

Comparison with calibration data from S5 and S6

The next step was to compare this data with the DARM gain data [2,4] from the S5 and S6 runs, which, as mentioned previously, also showed large discrepancies at the higher frequencies. We must keep in mind that the actual length control servo contains an ETM with a 2-degree vertical wedge at the AR surface, whereas our modelled optic is entirely symmetric. With the wedged optic, the maximum thickness is 100 mm, suggesting the optic may be a little less stiff. In that case, the slope of our ratio should be higher (Fig. 5) as the resonance happens earlier (for the LIGO ETMs, it is usually at 9.3 kHz). The radius of the actual magnet stand-offs is also slightly different [5]. We also do not take into account the resonance of the magnets in our model. A more realistic model that takes into account such asymmetries may show much larger discrepancies.

We plotted the HR surface data with the H1 DARM calibration data for the open loop gain (Fig. 5). It is apparent that test mass deformation cannot account fully for the measured calibration mismatch, which may further include contributions due to electronic filters that the raw data are subjected to, or, additional modifications in the deformation process arising from the optic wedge and/or glued magnets. These factors are rather relevant to the higher kHz, where precise measurements are much harder to achieve. We could still fit a function to the currently modelled profile and compensate for that in the calibration data. That way, we'd still be taking out some of the discrepancies.

Assessing mirror flexure for photon pressure actuation

In the final phase of this project, we investigated the flexure observed for a symmetrical configuration of photon pressure actuation (i.e., two forces). These forces—now acting on the HR surface, were aligned and placed about 34mm closer to the center than the OSEM setup. Our ratio plots revealed a significantly lower difference between the weighted measurements and the center of mass motion at 6kHz—a mere 5.6% difference at 6kHz. The AR surface flexed much more for this configuration of forces so the discrepancies were a little higher for the surface, around 8.5% (Fig. 6).

What could be causing such a huge difference between the two observations? We know that the only disparities between the two configurations are the number of force locales, their radial distance from the center of the optic and the circular area over which they act. Previously, we established that a small change in pressure due to slight variations in the radius of the circle has no profound effect on our observations.

We then investigated the deformations for four photon calibrator actuators (Fig. 6). We obtained profiles for the HR and AR surfaces that were very similar to the double actuator configuration; the difference between the corresponding plots amounted to about 0.2%; almost negligible (Fig. 6).

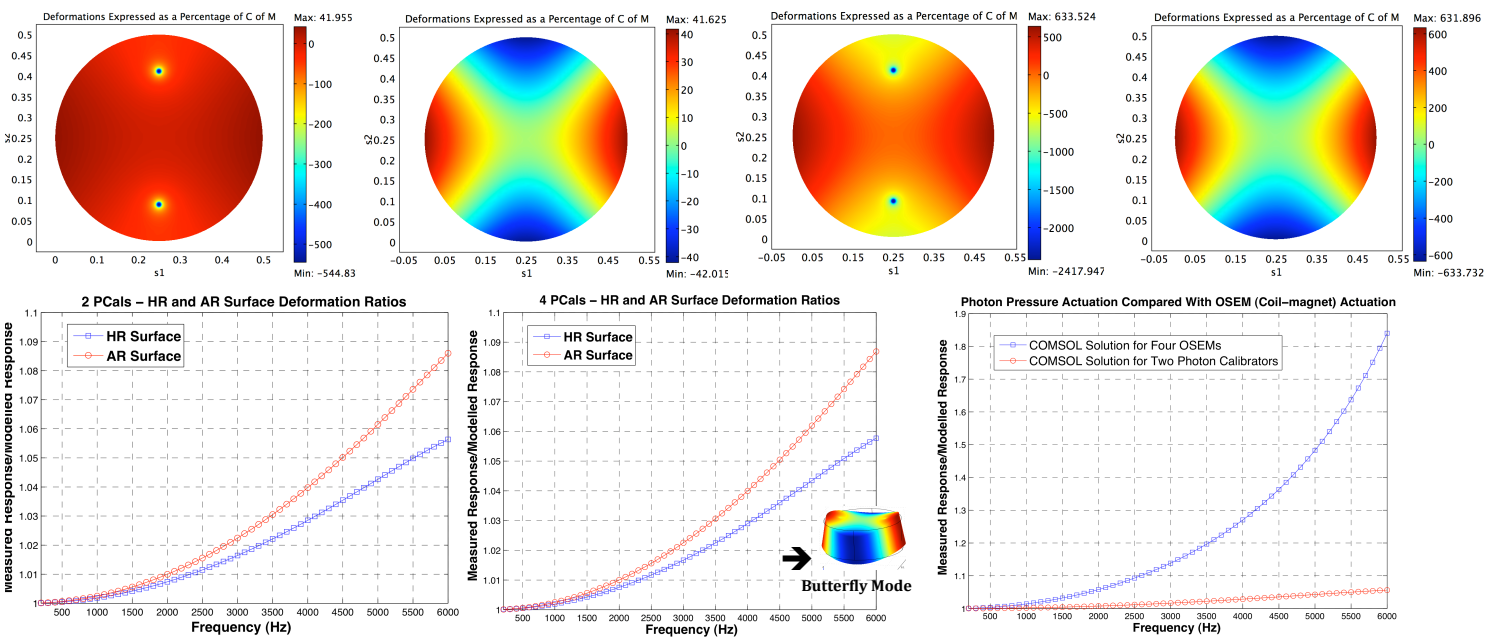

Figure 6| (Top) The HR (left) and AR (right) z-displacements for the photon actuation. The graphs show the 3D surface deformation as a percentage of the center of mass motion for 3 kHz and 6 kHz, respectively. (Bottom) The HR and AR surface Measured/Modelled Ratio profiles for the two photon calibrator forces, followed by four. The discrepancies experienced are about are about an order of magnitude less than the OSEM case for both configurations. This is because the optic flexes differently in perpendicular directions as they try to form the butterfly mode at 6823 Hz.

Tests of Force Radius and Beam Parameters

We further investigated the effect of varying the radial distance of the forces from the center of the optic. We carried out frequency response analysis for different radial distances. Deformation was found to be a function of the radial distance as well (Fig. 7).

This distance of minimum ratio increased as we moved radially outwards. If the forces were to be located within that distance, the optic flexure is out of phase with the center of motion. If they were located beyond, they would deform in phase with the center of mass motion, hence increasing the total displacements. The further these forces were, the longer their lever arm from the center is, and greater the effect of this flexure. Hence the ratio profiles for the OSEMs had significantly larger slopes than those for the photon calibrators, which were placed much closer to the center.

We also found for any symmetric force configuration, 82mm corresponds to the nodes of the drumhead mode. The phase and amplitude behaviour of the drumhead mode depends on how far the force locales are from this distance

and the relative direction (Fig. 7). If located beyond this distance, the force causes the center of the optic to first flex in phase with the center of mass motion and change sign as the driving frequency crosses the resonance point. Within this distance, the flexure is reversed. The further the force is from 82mm, the greater the maximum amplitude at the drumhead frequency.

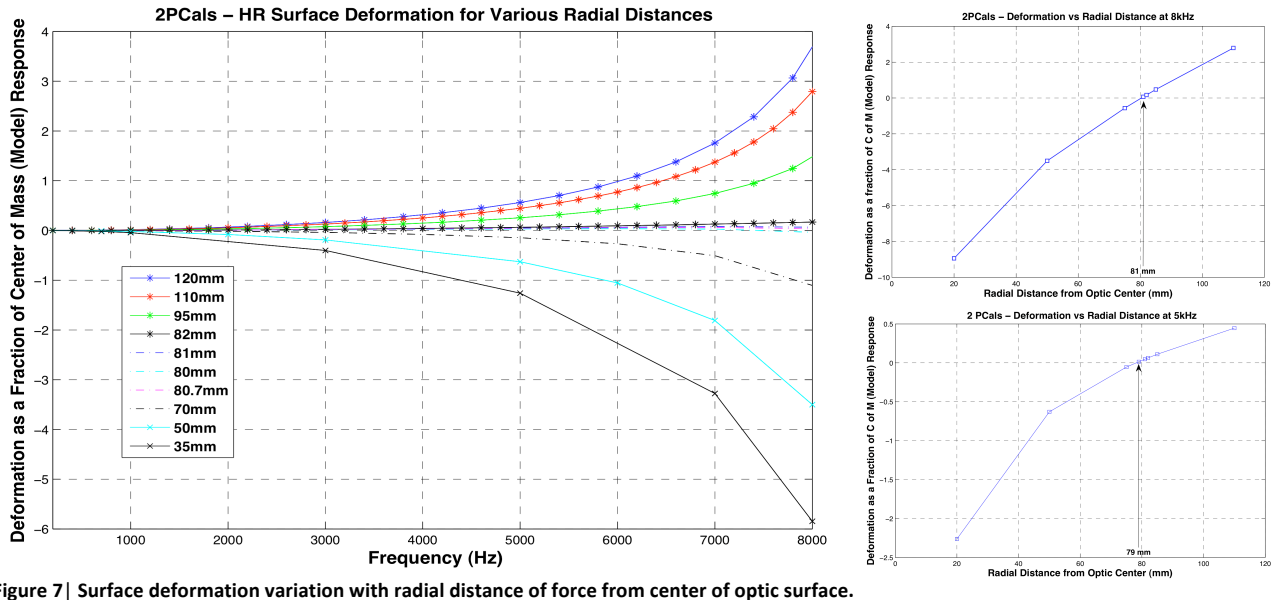

Figure 7| Surface deformation variation with radial distance of force from center of optic surface.

These observations clearly show some form of correlation between observed flexure behaviour and radial distance. The amplitude and phase of the deformations are evidently dependent on the radial distance of the forces from the center of the optic. This also tells us the distance we should aim the photon pressure actuators at to minimize our differences within the audio detection band.

We also extended our investigation to explore the effects interferometer beam radius and off centering of the beam. For an increasing beam radius, we'd expect a bias introduced by the dimples at the force locales, which would lower the value of the displacements weighted. We explored six different beam radii for three different radial distances and found the results to be consistent with the assumption. Since the optic is radially symmetric across either surface for the four OSEM configuration, the Gaussian weighting over an off-centered beam is also dependent on the radial distance. However, for the photon actuation case, the optic flexes one way on the diameter containing the forces and in the reverse way across the axis perpendicular to this line (Fig. 8). Hence the discrepancies observed are a little different depending on which way the beam is offset (Table 1).

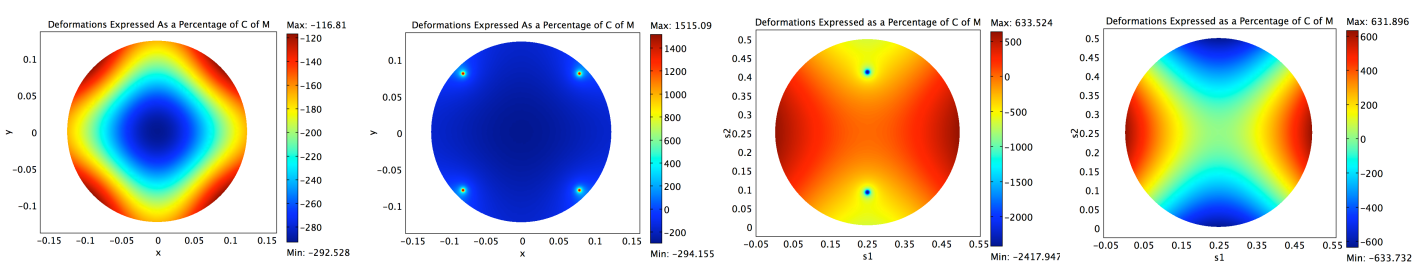

Figure 8| HR (left) and AR (right) Surface Displacement Patterns for OSEMs (left half) and Photon Calibrators (right half). Note that the sign convention has been reversed for the OSEMs have been reversed from Figure 1: red represents positive z values and vice versa for blue.

Measured as % of Modelled at 6 kHz (dw-fm/fm)	*OSEM Actuation*	*Photon Calibrator Actuation*
X=Y=0 (Beam is centered)	*84%*	*5.6%*
X=1, Y=0	*83%*	*11.2%*
X=0, Y=1	*83%*	*-1.3%*
X=1, Y=1 (Distance from Center = √2 mm)	*81.5%*	*4.5%*

Table 1| Results from off-centering the interferometer beam in both coil-magnet and photon calibrator actuation.

Summary and Future Work

Our results provided an explanation for the observed discrepancies in the H1 interferometer data. The amplitude and phase of the measured deformation were found to be function of the radial distance from center of test mass optic. We now have an idea of the distance to aim the photon pressure at in the future.

We anticipate some follow up work to be conducted in the near future that factor potentially significant asymmetries as i) the wedged optic and ii) glued standoff/magnet assemblies. A more realistic situation may yield a ratio profile for the coil-magnet actuators that better account for the discrepancies observed. It may then be necessary to carry out a more thorough analysis of the effects of off-centered beam. It would also be interesting to further explore the subject of optical stiffness. Finally, we'd like to incorporate the new ETM specifications into modeling an electrostatic drive such that we are able to probe the deformation of the Advanced LIGO optics.

METHOD

	Enhanced LIGO (eLIGO) End Test Mass Specifications [5] **(Symmetric)**	
Thickness (mm)	100 (thicker side in the vertically wedged optic)	
Diameter (mm)	250	
Material	Silica Glass	
Density (kg m^{-3})	2203	
Poisson Ratio	0.17	
Young's Modulus (GPA)	73.1 GPa	
Mechanical Loss	0.00001 (i.e. Q is 1e5)	
	Force Configuration Specifications [2,3,6]	
	OSEMs	Photon Calibrators
Size of Force (N)	1 per OSEM (i.e. 4N total)	2 per PCal (also 4N total)
Radius of Load Area (mm)	2	3
Separation	6.354", 6.364" (i.e. ~114.2 mm from surface center)	Mid-way between 2 OSEMs (i.e. 80.7 -or 80.8 mm depending on orientation- from center)
Placement (x, y, z coordinates)	(+/-0.0808, +/-0.0807, 0.0)	(0, 0.0807, 0.1), (0, -0.0807, 0.1)

Table 2| Enhanced LIGO ETM properties and the actuation parameters (initial) specified in the COMSOL models.

We acquired all of our modeling data using Structural Mechanics Module on COMSOL 3.5. Phil Willems had used the previous version for his initial modeling work [3], and the methods used to probe the deformations were adapted from the technical note. The only difference was that we did not have to export the displacements over a line segment across the radius at the surface, and multiply the individual surface displacement values in the z-direction (Fig. 1) with the Gaussian function $2/\pi\omega^2 \exp\left(\frac{-2(x^2+y^2)}{\omega^2}\right)$, in order to calculating the motion sensed by the interferometer beam [3,5].

We evaluated the displacements over the entire surface and used a "boundary integration coupling variable" that allowed us to multiply the individual mesh element displacements (parameter "w", representing the z-displacement values) by the Gaussian distribution function of the beam. The overlapping was calculated for a beam spot size of ω = 3.4 cm, centrally situated at the surface of the optic. Note that all we needed to do to move the beam off-center and change the size of the beam was to parameterize the Gaussian function accordingly. Every time this expression is modified, it becomes necessary to resolve the model. The solver must also be restarted for any change involving the geometry and object properties.

The center of mass motion, at any frequency, was obtained by integrating the z-displacement values over the entire optic, and then dividing out the volume of the optic. This ensured that we were averaging the individual motion of each mesh element [3]. The COMSOL calculated value was found to be, at most, 0.015% different from the value we obtain using the rigid body formula for a free mass:

$$Xz = \frac{F}{(2\pi f)^2 m} \quad \text{or} \quad Xz = \frac{2P}{(2\pi f)^2 mc} \quad (P = \text{laser power})$$

Note that we used a force of 1 N per OSEM to keep the input unitary. The force factors out in the calculations, and so our ratios must be independent of the force. To find the displacements corresponding to any force or laser power, we would only need to scale our data accordingly. For the LIGO interferometers, our finite-element models predict length variations in the order of 10^{-19} to 10^{-18} m for photon calibrator actuation, and ~10^{-17} m for coil-magnet actuation.

The data was extracted from the model using the extensive post-processing options built into COMSOL that allow both 2D and 3D plots across any desired cross-section or surface. We exported the data into MATLAB and obtained our plots and tables.

At the beginning of the investigation, we had used steady-state modeling to probe the flexure-induced deformations. Although the frequency response modeling work depicted the actual optic behaviour, steady-state models allowed us to look into the optic without the added complication of inertial restoration. We had applied an equal and opposite force to the entire optic that suppressed the bulk recoil motion. This force allowed us to run a static model to look at the deformation for low frequency applied forces without having the mirror run away in model space due to the actuation forces. In effect, we were using this equal and opposite force to stand in for the inertia.

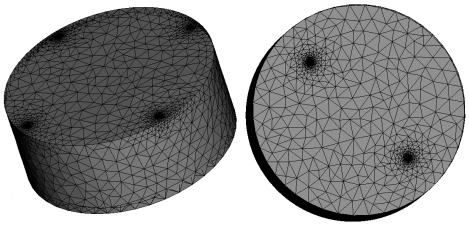

Figure 9| Customized mesh resolutions for both force configurations.

We also used the default settings in the mesh parameter menu for defining the lattice points throughout the optic, while custom refining the resolution of the meshing at the boundary regions containing the forces. Since our forces were applied over radii in the mm range, we specified the maximum element size of a mesh grid to be 1 mm at these regions. For the 82 mm node distance, we had to further refine it (0.5 mm) to be able to correctly resolve the node points. We even tried custom meshing across line segments and using the fine/finer settings on the main mesh window to see if it makes any notable difference to our ratio values. The result was negative.

[1] Hild S., Photon Pressure Induced Test Mass Deformation in Gravitational-Wave Detectors. *Class. Quantum Grav*. **24** 5681-5688 (2007).
[2] L Michael, private communication.
[3] Willems, P., Finite Element Modeling of Test Mass Flexure Laboratory/LIGO Scientific Collaboration. *LIGO Technical Document* T080190-00-R available from http://admdbsrv.ligo.caltech.edu/dcc (2008).
[4] K Kawabe, private communication.
[5] Kawamura S., Hazel J., Barton M., Large Optics Suspension Final Design (Mechanical System). *LIGO Technical Document* T970158-06-D available from http://admdbsrv.ligo.caltech.edu/dcc (1997).
[6] R Savage, private communication.

Acknowledgments The authors gratefully acknowledge the support of the United States National Science Foundation for the construction and operation of the LIGO Laboratory and the Science and Technology Facilities Council of the United Kingdom, the Max-Planck-Society, and the State of Niedersachsen/Germany for support of the construction and operation of the GEO600 detector. The authors thank the LIGO calibration team, Jeff Kissel and Jonathan Hanks, General Computing System Administrator at the LIGO Hanford Observatory, for their valuable contribution. The authors also gratefully acknowledge the support of the research by these agencies and by the Australian Research Council, the Council of Scientific and Industrial Research of India, the Instituto Nazionale di Fisica Nucleare of Italy, the Spanish Ministerio de Educacion y Ciencia, the Conselleria d'Economia Hisenda i Innovacio of the Govern de les Illes Balears, the Royal Society, the Scottish Funding Council, the Scottish Universities Physics Alliance, The National Aeronautics and Space Administration, the Carnegie Trust, the Leverhulme Trust, the David and Lucile Packard Foundation, the Research Corporation, and the Alfred P. Sloan Foundation. This document has been assigned LIGO Laboratory document number LIGO-T0900401.